Image Anal Stereol 2026;45:51-63 doi: 10.5566/ias.3900
Original Research Paper

ESTIMATION OF THE PAIR CORRELATION FUNCTION OF RANDOM POINT FIELDS VIA FREQUENCY DOMAIN

JOACHIM OHSER

Dept. of Math. & Nat. Sci., University of Applied Sci., Schöfferstraße 3, D-64295 Darmstadt, Germany
e-mail: joachim@ohser-online.de
(Received January 29, 2026; revised March 19, 2026; accepted March 19, 2026)

ABSTRACT

Applying a Wiener-Khintchine type theorem for random point fields, the estimation of the pair correlation function via the frequency domain is presented, which offers certain advantages over conventional estimation, especially for large datasets. The discretization of the point data, i.e., its mapping onto a grid, can be viewed as a digital image, where this mapping includes regularization of the data. Using a fast Fourier transform and its co-transform, the estimation of the pair correlation is consistently embedded in the field of digital image analysis. Finally, building upon this technique, an estimator of the density of the Bartlett spectrum is derived, whose normalization is known in scattering theory as the structure factor. The suitability of the estimators is demonstrated with examples.

Keywords: image analysis, random point field, spatial statistics, structure factor.

INTRODUCTION

The pair correlation function (PCF) is perhaps the most important characteristic of macroscopically homogeneous random point fields (besides intensity, i. e., the mean number of points per unit volume). There are well-established methods for estimating the PCF, which essentially date back to Ripley (1976) and have been modified in numerous publications with regard to the treatment of edge effects resulting from data windowing, regularization (smoothing), normalization, etc. Applications range from characterizing the distribution of atom sites in amorphous materials, over quantifying the arrangement of non-metallic inclusions in steels, dense particle packings in powders and bulk materials, to determining features of plant locations in biotopes or positions of galaxies in space.

Sometimes the radial distribution function (RDF), the K-function, or the L-function are used instead of the PCF. These functions can be represented as integrals of the PCF, with the integration contributing to the regularization of estimates. These quantities essentially contain the same information about the point pattern as the PCF. This is also true for the spectral measure of point fields pioneered by Maurice Stevenson Bartlett (Bartlett, 1963; 1964), known as the *Bartlett spectrum*. The density of the Bartlett spectrum (if it exists) can be interpreted in a similar way as the intensity of radiation scattering, which can be determined using physical techniques, e.g., small-angle scattering (SAS) or scanning small angle scattering (sSAS) of X-rays, electrons, neutrons or beta radiation. Consequently, suggestions from the physical interpretation of scattering experiments can be transferred to the interpretation of the density of the Bartlett spectrum.

The problem of estimating second-order quantities of point processes, namely the PCF and the structure factor, is revisited, now arguing from the perspective of digital image analysis and emphasizing computational aspects, with the fast Fourier transform being the core of the algorithms.

Based on a Wiener-Khintchine type theorem for random closed sets, a method for estimating their second-order product densities via spatial frequency domain was derived in Koch (2002); Koch *et al.* (2003); Ohser *et al.* (2005). In the present article, this approach is applied to random point fields, which are nothing more than special cases of random sets. However, estimating the PCF via the frequency domain involves solving additional problems inherent to point fields, including the need for appropriate discretization. The basic idea is to map a point pattern onto a grid. Such a mapping can be interpreted as a digital image. Hence, the estimation of the second-order product density can be considered as a problem of digital image analysis, which is consistent as e. g. the centers of mass of objects arising in image analysis are forming random point patterns, too. A fast Fourier transform contributes to the efficiency of an estimation algorithm. For large point samples, this is a significant computational advantage over conventional estimators, whose complexity is of the order of the squared point number of the sample. Furthermore, our approach enables a simultaneous computation of the window function (also known as the apodization

function or tapering function) for arbitrarily shaped compact windows, allowing for precise correction of edge effects.

The article is organized as follows: First, two important second-order characteristics of macroscopically homogeneous point fields are introduced: the PCF and its counterpart in the frequency domain – the so called structure factor (Coppens, 2006) that plays a major role, e. g. in the interpretation of scattering experiments (Walters *et al.*, 1993). Then, two estimators of the PCF are presented: the conventional Fiksel estimator (Fiksel, 1988) and the estimation via frequency domain. Furthermore, an estimator of the structure factor is given, that incorporates multiple transitions between real domain and frequency domain. Finally, the suitability of the presented estimators is demonstrated using examples of random point fields: the sites of the extremal points of Berry's random wave (Estrade and Fournier, 2024) and the centers of the carbon black particles in rubber (Le *et al.*, 2008).

SECOND-ORDER PROPERTIES OF POINT FIELDS

Let $(\Omega,\mathcal{A},\mathbb{P})$ be a probability space and $\mathcal{N}$ be the σ-algebra generated by the set of all locally finite counting measures $\mathcal{N}'$ on $\mathbb{R}^d$. Then a random point field in $\mathbb{R}^d$ is a measurable mapping Φ from a probability space $(\Omega,\mathcal{A},\mathbb{P})$ to the measurable space $(\mathcal{N}',\mathcal{N})$. The first- and second-order properties of Φ can be expressed in terms of the intensity measure Λ and the reduced second-order measure $\mathcal{K}$, respectively (Daley and Vere-Jones, 1988). When interpreting Φ as a counting measure, the intensity measure is defined as the expectation $\Lambda(B)=\mathbb{E}\Phi(B)$ for all Borel sets, $B\in\mathcal{B}(\mathbb{R}^d)$.

PAIR CORRELATION FUNCTION

For simplicity we assume that Φ is simple and locally finite. If Φ is additionally macroscopically homogeneous (stationary), i. e. the image measure of Φ is motion invariant, then the intensity measure Λ is absolute continuous with respect to the Lebesgue measure ν. There exists a density $\lambda>0$ of Λ with $\Lambda=\lambda\nu$, called the point density or the mean number of points per unit volume. Moreover, the second reduced moment measure $\mathcal{K}$ of a second-order point field Φ is absolute continuous with respect to ν, which means that there exists a density function $g:\mathbb{R}^d\mapsto\mathbb{R}$ with

$$\mathcal{K}(B)=\int_B g(x)\,\nu(dx),\qquad B\in\mathcal{B}(\mathbb{R}^d),$$

where $\lambda\mathcal{K}(B)$ is the mean number of points in $B\setminus\{0\}$ given that 0 is a point of Φ (Chiu *et al.*, 2013). The function g is called the pair correlation function (PCF) of Φ (also known as the two-point correlation). If the point field Φ is macroscopically isometric, i. e. if it is not only macroscopically homogeneous but also isotropic, then the function g depends on only the radial coordinate $r=\|x\|$ of x, and there exists a function $\bar{g}(r)$, such that $\bar{g}(\|x\|)=g(x)$ for all $x\in\mathbb{R}^d$.

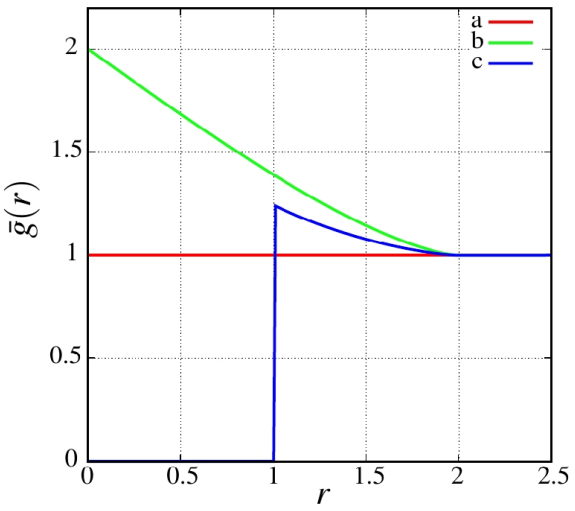

Fig. 1. *The PCF $\bar{g}(r)$ for $d=2$: a) Poisson point field, b) Matérn's cluster point field for $\lambda=\lambda_C=1$, c) Matérn II hard-core point field for $\lambda=1/\pi$*

Poisson point field. The standard model of the point field theory, i. e. the macroscopically homogeneous Poisson point field, has the property that the number of points in a bounded window is a Poisson-distributed random variable and the point sites are pairwise independent and uniformly distributet in the window. The PCF is constant,

$$g(x)=1,\qquad x\in\mathbb{R}^d$$

(Chiu *et al.*, 2013).

Matérn's cluster point field. A further very simple example is Matérn's cluster point field (Matérn, 2013; Chiu *et al.*, 2013) with the unit ball $B=\{x\in\mathbb{R}^d:\|x\|\le 1\}$ as the clusters. Let λ_C be the cluster density (i. e. the mean number of clusters per unit volume), and let λ_P be the point density inside the clusters, then the point density λ of Matérn cluster point field is $\lambda=\lambda_C\lambda_P\nu(B)$ with the volume $\nu(B)$ of the unit ball B. Then the PCF of Matérn's cluster point field is given by

$$g(x)=\frac{\lambda_C}{\lambda}\frac{c_B(x)}{\nu(B)}+1,\qquad x\in\mathbb{R}^d,\qquad(1)$$

where $c_B(x) = \nu(B \cap B+x)$ is the set covariance of B (Chiu *et al.*, 2013). Similar to the above, we are setting $\bar{c}_B(\|x\|) = c_B(x)$. In the 2D case we have

$$\bar{c}_B(r) = 2\arccos\frac{r}{2} - r\sqrt{1-\frac{r^2}{4}}, \qquad 0 \le r \le 2,$$

and $\bar{c}_B(r) = 0$ for $r > 2$. In the 3D case, it is

$$\bar{c}_B(r) = \frac{4\pi}{3}\left(1 - \frac{3}{4}r + \frac{1}{16}r^3\right), \qquad 0 \le r \le 2,$$

and $\bar{c}_B(r) = 0$ otherwise.

Matérn II hard-core point field. Finally, we consider the Matérn II hard-core point field (Matérn, 2013; Chiu *et al.*, 2013) with the point density λ_P of the underlying Poisson point field and the hard-core distance $h = 1$. For $\lambda_P \to \infty$, the point density λ of the Matérn II hard-core point field is $\lambda = 1/\nu(B)$, and the PCF is given by

$$g(x) = \begin{cases} 0, & 0 \le \|x\| \le 1 \\ \dfrac{2}{2 - \lambda c_B(x)}, & 1 < \|x\| \le 2 \\ 1, & \|x\| > 2 \end{cases}.$$

Fig. 1 shows the graphs of the PCF for the point field examples mentioned above.

BARTLETT SPECTRUM

We follow the the ideas of Bartlett (1963; 1964; 1975); Vere-Jones (1974) and remember the foreword to the first edition of the book by Stoyan *et al.* (1985) in which David Kendall stated: *"What we now call stochastic geometry began for me with the papers of Maurice Bartlett ... ".*

Let $\mathscr{S}(\mathbb{R}^d)$ be the Schwartz space, i. e. the set of all functions of rapid decay, and let Φ be a macroscopically homogeneous and second-order point field. By Proposition 11.2.I of Daley and Vere-Jones (1988) there exists a unique measure Γ_Φ associated with Φ such that

$$\operatorname{var} \int_{\mathbb{R}^d} \psi(x)\, \Phi(dx) = \int_{\mathbb{R}^d} \left|\hat{\psi}(\xi)\right|^2 \Gamma_\Phi(d\xi) \qquad (2)$$

for all $\psi \in \mathscr{S}(\mathbb{R}^d)$, where $\hat{\psi}(\xi)$ is the Fourier transform of $\psi(x)$, i. e.

$$\hat{\psi}(\xi) = \frac{1}{(2\pi)^{\frac{d}{2}}} \int_{R^d} \psi(x)\, \mathrm{e}^{-ix\xi}\, dx, \quad \xi \in \mathbb{R}^d,$$

for short $\hat{\psi}(\xi) = \big(\mathscr{F}\psi\big)(\xi)$. The measure Γ_Φ is called the *Bartlett spectral measure* or shortly the *Bartlett spectrum* of Φ.

The density γ of Γ_Φ – if it exists – is called the *power spectral density* (PSD); it writes $\gamma(\xi)\, d\xi = \Gamma_\Phi(d\xi)$. Notice that the PSD $\gamma(\xi)$ is a scaled quantity; the unit is m^d while x is in m and the circular frequency ξ is in m^{-1}. In scattering theory, ξ is called the *wave vector* and the unscaled function

$$s(\xi) = (2\pi)^{d/2}\, \lambda\, \gamma(\xi), \qquad \xi \in \mathbb{R}^d$$

is the *statistic structure factor* (or shortly *structure factor*) of the field of atom sites (Walters *et al.*, 1993; Massaro and del Campo, 2025). It is widely used to describe the scattering intensity of radiation at macroscopically homogeneous microstructures. More precisely, $s(\xi)$ relates the observed diffracted intensity per atom to the total intensity emitted by a single scattering unit.

The structure factor is related to the PCF by the relationship

$$s(\xi) = \lambda \int_{\mathbb{R}^d} \big(g(x) - 1\big)\, \mathrm{e}^{-ix\xi}\, dx + 1, \qquad \xi \in \mathbb{R}^d$$

(Walters *et al.*, 1993). In the isotropic case, the PSD depends only on the radial coordinate $\rho = \|\xi\|$ of the circular frequency ξ, i. e. there is a function $\bar{\gamma}(\rho)$ such that $\bar{\gamma}(\|\xi\|) = \gamma(\xi)$. Analogously, we are setting and $\bar{s}(\|\xi\|) = s(\xi)$, where $\bar{s}(\rho) - 1$ is basically the Fourier-Bessel transform of $\bar{g}(r) - 1$, i. e. a linear integral transform whose kernel consists of the Bessel functions J_μ of the first kind and of order μ (Poularikas, 2000, Chapter 9.11). More precisely,

$$\bar{s}(\rho) = \frac{\lambda}{\rho^{\frac{d-2}{2}}} \int_0^\infty \big(\bar{g}(r) - 1\big)\, r^{\frac{d}{2}}\, J_{\frac{d-2}{2}}(r\rho)\, dr + 1, \quad \rho \ge 0.$$

Notice that the Fourier-Bessel transform is also known as the Hankel transform and for $d = 2$ resp. $d = 3$ it is the ordinary Bessel transform resp. the sine transform. For scattering of γ-, β- or X-rays of incident wave length λ_0 at a liquid or an amorphous material, the quantity $\rho = (4\pi/\lambda_0)\sin\theta$ is called the wave vector transfer, where θ is called the glancing angle and 2θ is said to be the scattering angle (Kittel, 2018, Chapter 3).

Poisson point field. The macroscopically homogeneous Poisson point field has a constant structure factor,

$$\bar{s}(\rho) = 1, \qquad \rho \ge 0.$$

Since white noise also has a constant power spectral density (Jähne, 2005), the Poisson point field is sometimes called the white noise point field.

Matérn cluster point field. For the 2D Matérn cluster point field in the above setting, the structure factor can be given in a closed form. The ordinary Bessel transformation of the indicator function $\mathbf{1}_{[0,1]}(r)$ of the interval $[0,1]$ is

$$\int_0^2 r\mathbf{1}_{[0,1]}(r)J_0(r\rho)\,dr = \frac{J_1(\rho)}{\rho}, \quad \rho \geq 0$$

(Oberhettinger, 1972), where we remark that $J_1(\rho)/\rho \to \frac{1}{2}$ as $\rho \to 0$. Now, from the convolution theorem of Fourier transform, it immediately follows that the Bessel transform of the set covariance function $\bar{c}_B(r)$ is given by

$$\int_0^2 r\bar{c}_B(r)J_0(r\rho)\,dr = 2\pi\frac{J_1^2(\rho)}{\rho^2}, \quad \rho \geq 0.$$

Finally, from Eq. 1 one gets

$$\bar{s}(\rho) = 2\frac{\lambda_C}{\lambda}\frac{J_1^2(\rho)}{\rho^2} + 1, \qquad \rho \geq 0.$$

In the 3D case, the sine transform yields

$$\sqrt{\frac{2}{\pi}}\frac{1}{\rho}\int_0^2 \bar{c}(r)\,r\sin r\rho\,dr = 4\sqrt{2\pi}\left(\frac{\sin\rho}{\rho^3} - \frac{\cos\rho}{\rho^2}\right)^2$$

for $\rho \geq 0$, where $(\sin\rho/\rho^3 - \cos\rho/\rho^2) \to \frac{1}{3}$ as $\rho \to 0$. Thus we get

$$\bar{s}(\rho) = 3\frac{\lambda_C}{\lambda}\sqrt{\frac{2}{\pi}}\left(\frac{\sin\rho}{\rho^3} - \frac{\cos\rho}{\rho^2}\right)^2 + 1, \quad \rho \geq 0.$$

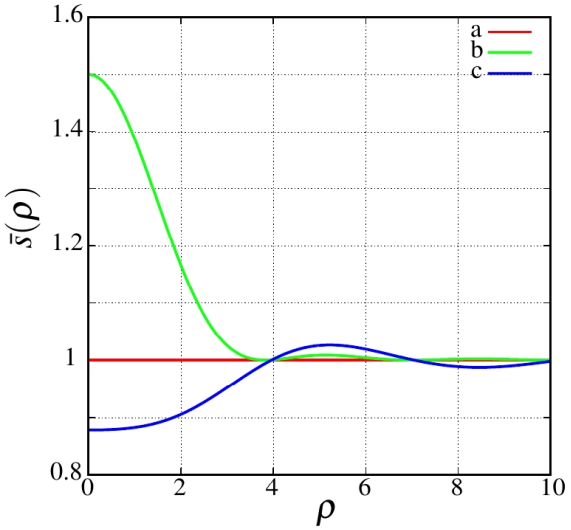

Fig. 2. *The structure factor $\bar{s}(\rho)$ of 2D point fields:*
a) Poisson point field,
b) Matérn's cluster point field for $\lambda = \lambda_C = 1$,
c) Matérn II hard-core point field for $\lambda = 1/\pi$

Matérn II hard-core point. Unfortunately, the structure factor of the Matérn II hard-core point field can not be given in a closed form. The Bessel transformation of the indicator function $\mathbf{1}_{[0,1]}(r)$ is

$$\bar{s}(\rho) = \lambda^2\int_1^2 \frac{r\bar{c}_B(r)}{2-\lambda\bar{c}_B(r)}J_0(r\rho)\,dr - \frac{J_1(\rho)}{\rho} + 1,$$

for $\rho > 0$. The graph of the structure factor $\bar{s}(\rho)$ is shown in Fig. 2. In the 3D case, the graph of $\bar{s}(\rho)$ has a similar shape.

For further details on the spectral measure of random point fields and various applications (e. g. in plasma physics, archaeology, forestry and astronomy) we refer to Graham (1980); Brémaud and Massoulié (2002); Gabrielli and Torquato (2004); Prémaud *et al.* (2005); Brémaud (2014); Hawat *et al.* (2023); Grainger *et al.* (2025). In Rajala *et al.* (2023) one can find closed-form expressions for the structure factor of other models of point fields, including special cases of Thomas' cluster point fields. One should also pay attention to Coulomb gas, i. e. a random system of charged particles interacting under the electrostatic force, whose structure factor is frequently discussed in theoretical physics, see e. g. Boudjemâa (2023).

ESTIMATION OF THE SECOND-ORDER CHARACTERISTICS

In this section, we first present a conventional estimator of the isotropic PCF $\bar{g}(r)$ in point field statistics. Then, we introduce an estimator of $g(x)$ based on the application of Fourier methods. As we will see, this type of PCF estimation via the frequency domain proves to be an intermediate step in the estimation of the structure factor $s(\xi)$.

CONVENTIONAL ESTIMATION OF THE PAIR CORRELATION FUNCTION

Let $x_1,\ldots,x_m$, $m > 1$, be a sample of an isotropic point field Φ observed in a compact window $W \subset \mathbb{R}^d$ with nonempty interior and the rotation average $\bar{c}_W(r)$ of the window function $c_W(x) = \nu(W \cap W + x)$, i. e.

$$\bar{c}_W(r) = \frac{1}{\omega_d}\int_{S^{d-1}} c_W(r\theta)\,\mu(d\theta), \quad r \geq 0,$$

where x is given in spherical polar coordinates $x = r\theta$ with $r = \|x\|$ and $\theta = x/r \in S^{d-1}$ for $r > 0$, and μ is the Lebesgue measure on the unit sphere S^{d-1} with $\omega_d = \mu(S^{d-1})$. Furthermore, let $\kappa_\sigma : \mathbb{R} \mapsto \mathbb{R}$ be a positive kernel function of bounded support and with

$\int_{\mathbb{R}} \kappa_\sigma(r)dr = 1$. The parameter σ is the kernel width. Then the PCF $\bar{g}(r)$ can be estimated using

$$\tilde{\bar{g}}(r) = \frac{2v^2(W)}{\lambda^2 \omega_d \bar{c}_W(r)} \sum_{i=1}^{m-1} \sum_{j=i+1}^{m} \kappa_\sigma\big(\|x_i - x_j\| - r\big), \quad (3)$$

for all r with $\bar{c}_W(r) > 0$, where the unknown λ^2 is replaced with the usual estimator $\widetilde{\lambda^2} = m(m-1)/v^2(W)$ which is unbiased for Poisson point fields. This estimator was first suggested by Fiksel (1988) with κ_σ being the Epanechnikov kernel.

It can easily be seen that the complexity of the estimator given by Eq. 3 is of order $\mathcal{O}(m^2)$ for each discrete value of r, i. e. the estimation is time consuming for large point samples. However, quick sorting of the point distances and the boundedness of the kernel's support can significantly speed up the estimation procedure. A second point is that the smoothing with the kernel is performed in the distance domain, where point distances occur with different frequencies. Therefore, the kernel width σ and thus the strength of smoothing must be adapted to the varying frequencies. This could be a challenge, since these frequencies depend on the point field itself and the window shape. Finally, it should be noted that in the case of an irregularly shaped window W, i. e. if W is neither a ball nor a cuboid, a straightforward computation of the window function $\bar{c}_W(r)$ may be difficult. Source code of computing $\bar{c}_W(r)$ is given e. g. by Ohser and Mücklich (2000), p. 356f for spherical resp. cuboidal windows.

Variants of Fiksel's kernel estimator are discussed e. g. in Baddeley *et al.* (2015), which lead to a significant reduction in systematic and statistical errors in estimation. This includes local adaptive smoothing of the estimate and modified edge correction. Furthermore, Baddeley *et al.* (2025) pays particular attention to improved estimation of the PCF for small distances. However, the complexity of the algorithms behind the estimators remains unchanged.

ESTIMATING THE PAIR CORRELATION FUNCTION VIA FREQUENCY DOMAIN

In contrast to the above, we start with a smoothing, namely the smoothing of the point field Φ with a non-negative kernel $\kappa : \mathbb{R}^d \mapsto \mathbb{R}$ satisfying $\int_{\mathbb{R}^d} \kappa(x)dx = 1$. Let denote κ^* the reflection of κ at the origin, i. e. $\kappa^*(x) = \kappa(-x)$ for all $x \in \mathbb{R}^d$, then the convolution

$$\kappa_2(x) = \big(\kappa * \kappa^*\big)(x) = \int_{\mathbb{R}^d} \kappa(y)\kappa(y-x)dy, \quad x \in \mathbb{R}^d$$

is symmetric and $\int_{\mathbb{R}^d} \kappa_2(x)dx = 1$. Furthermore, if κ is of compact support, then so is $\kappa * \kappa^*$.

We introduce a random function $f : \Omega \times \mathbb{R}^d \mapsto \mathbb{R}$ given by

$$f = (\Phi - \mathbb{E}\Phi) * \kappa \quad (4)$$

and its restriction $f_W(x) = f(x)\mathbf{1}_W(x)$ to a compact window $W \subset \mathbb{R}^d$, where $\mathbf{1}_W(x)$ is the indicator function of W, i. e. $\mathbf{1}_W(x) = 1$ if $x \in W$, and $\mathbf{1}_W(x) = 0$ otherwise. From Campbell's theorem (Daley and Vere-Jones, 1988, p. 188) it follows that f is measurable and, hence, it defines a stochastic process with the expectation $\mathbb{E}f(x) = 0$ for all $x \in \mathbb{R}^d$ and the covariance function

$$\mathrm{cov}_f(x) = \mathbb{E}f(y)f(y+x), \qquad x, y \in \mathbb{R}^d.$$

If the PCF $g(x)$ is locally integrable, then the covariance function can be rewritten as

$$\mathrm{cov}_f(x) = \lambda\kappa_2(x) + \lambda^2 \int_{\mathbb{R}^d} \kappa_2(y)g(y-x)\,dy - \lambda^2 \quad (5)$$

for $x \in \mathbb{R}^d$, where the integral is a convolution since κ_2 and g are even. In other words, up to constants and the central reflex $\lambda\kappa_2$, the covariance function is a smoothed version of the PCF.

Now we chose a κ such that $\Phi * \kappa$ almost surely is a substantially bounded function. Then f is almost surely locally integrable and f_W is almost surely integrable. The Fourier transform $\hat{f}_W(\xi) = \big(\mathscr{F} f_W\big)(\xi)$ of $f_W(x)$ exists, and one obtains the relationship

$$(2\pi)^{d/2}\mathbb{E}\big|\hat{f}_W(\xi)\big|^2 = \mathscr{F}\big(c_W \mathrm{cov}_f\big)(\xi), \quad \xi \in \mathbb{R}^d,$$

which follows from the Wiener-Khintchine theorem (Ohser and Schladitz, 2009, Theorem 6.3). We apply the inverse Fourier transform $\bar{\mathscr{F}}$ to the expectation $\mathbb{E}|\hat{f}_W(\xi)|^2$ written as

$$\bar{\mathscr{F}}\mathbb{E}|\hat{f}_W|^2(x) = \frac{1}{(2\pi)^{d/2}} \int_{\mathbb{R}^d} \mathbb{E}|\hat{f}_W(\xi)|^2 \mathrm{e}^{ix\xi}\,d\xi$$

for all $x \in \mathbb{R}^d$, and together with Eq. 5 one obtains

$$\begin{aligned}(2\pi)^{d/2}\bar{\mathscr{F}}\mathbb{E}\big|\hat{f}_W\big|^2(x) &= \big(c_W \mathrm{cov}_f\big)(x) \quad (6)\\ &= \lambda\big(c_W\kappa_2\big)(x) + \lambda^2\big(c_W(\kappa_2 * g)\big)(x) - \lambda^2 c_W(x)\end{aligned}$$

for $x \in \mathbb{R}^d$. Finally, rearranging the last equation for the desired function $\kappa_2 * g$ yields

$$\big(\kappa_2 * g\big)(x) = (2\pi)^{d/2}\frac{\bar{\mathscr{F}}\mathbb{E}\big|\hat{f}_W\big|^2(x)}{\lambda^2 c_W(x)} - \frac{\kappa_2(x)}{\lambda} + 1 \quad (7)$$

for all x in the interior W° of the window W. For a kernel κ of decreasing width the left-hand side of

the last equation converges to $g(x)$. More precisely, let $\{\kappa_a\}_{a>0}$ be a family of non-negative functions on $\mathbb{R}^d$ of compact support. If $\|\kappa_a\|_{L^1} = 1$ for all $a > 0$ and $\kappa_a(x) = 0$ for all $x \in \mathbb{R}^d$ with $\|x\| > a$ then

$$\big((\kappa_a * \kappa_a^*) * g\big)(x) \to g(x) \quad \text{as} \quad a \to 0$$

for those $x \in \mathbb{R}^d$ where g is continuous. In this sense

$$\tilde{g}(x) = (2\pi)^{d/2} \frac{\bar{\mathscr{F}}\big|\hat{f}_W\big|^2(x)}{\lambda^2 c_W(x)} - \frac{\kappa_2(x)}{\lambda} + 1$$

is an asymptotically unbiased estimator of $g(x)$ for all $x \in W^\circ$. We replace the unknown intensity λ with $m/\nu(W)$, and λ^2 is replaced with $m(m-1)/\nu^2(W)$.

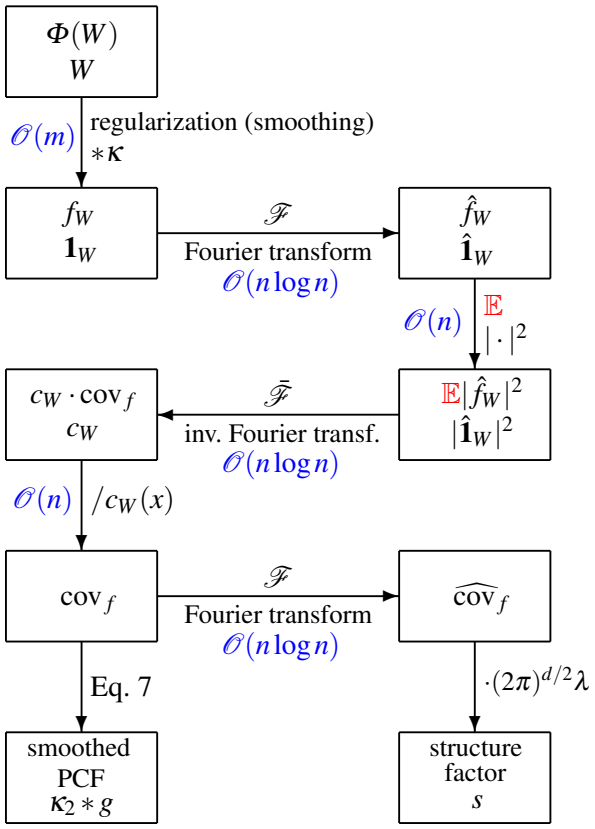

Fig. 3. *Scheme of computing the smoothed PCF* $\big(\kappa_2 * g\big)(x)$ *and the structure factor* $s(\xi)$*, respectively.*

Let $\mathbb{Z}$ be the set of integers and let $a\mathbb{Z}^d$ be a cubic lattice of spacing $a > 0$ and with the closed and half-open unit cells $C = [0,a]^d$ and $C' = [0,a)^d$, respectively. For the sake of simplicity, let us first assume that the window W is cuboidal. In the language of image processing $C + x$ for $x \in a\mathbb{Z}^d \cap W$ are the pixels (voxels) of an image of the pixel size a. Then the random function f is chosen as the sampling of the point field Φ on $a\mathbb{Z}^d$,

$$f(x) = \frac{1}{a^d}\Phi(C' + x) - \lambda, \quad x \in \mathbb{R}^d,$$

where we note that the function $f(x)$ is the same as that given by Eq. 4 for $\kappa(x) = \mathbf{1}_C(x)/a^d$. Here, the pixel size a corresponds to the kernel width; it serves as a regularization of estimation. Fig. 3 shows a sketch of the computation, where $\hat{\mathbf{1}}_W$ denotes the Fourier transform of the indicator function $\mathbf{1}_W$.

Finally, the continuous Fourier transform $\mathscr{F}$ and its co-transform $\bar{\mathscr{F}}$ are replaced by their discrete ones, where we have to take into consideration that discrete Fourier transforms usually inherit a periodic continuation of f_W with respect to the window W. This causes data overlapping that can be avoided by expanding the function f_W to the window $2W$ in the following way: Instead of f_W we use the function f_{2W} defined as $f_{2W}(x) = f(x)$ for $x \in W$ and $f_{2W}(x) = 0$ for $x \in 2W \setminus W$. Then a discrete Fourier transform of f_{2W} is the same as that of f. Analogously, we proceed for computing the window function $c_W(x)$ from indicator function $\mathbf{1}_W(x)$ via frequency domain, where $\mathbf{1}_W(x)$ is replaced with $\mathbf{1}_{2W}(x)$.

When applying a fast Fourier transform (FFT) and its co-transform, then the estimation algorithm presented in Eq. 7 is of order $\mathscr{O}(n \log n)$, where n is the number of pixels of the sampling $W \cap a\mathbb{Z}^d$ of the window W on the lattice $a\mathbb{Z}^d$. A scheme of estimating the PCF via frequency domain is shown in Fig. 3, also indicating the complexity of the substeps of the estimation procedure. For a large point number m, estimation via frequency domain is more time consuming than conventional estimation using Eq. 3.

The scheme in Fig. 3 already inherits the computation of the window function $c_W(x)$ via frequency domain, where we point out that in the case of a cuboidal window, the window function can easily be calculated without any help of Fourier transform. However, if W is not a cuboid (or a ball), then a careful data windowing is generally very expensive and, thus, we proceed as follows: Let $W_\square$ be the smallest cuboidal window containing W, $W_\square \subseteq W$. Then we replace f_{2W} with $f_{2W_\square}$ defined as $f_{2W_\square}(x) = f(x)$ for $x \in W$ and $f_{2W_\square}(x) = 0$ for $x \in 2W_\square \setminus W$. Furthermore, we replace $\mathbf{1}_{2W}(x)$ with $\mathbf{1}_{2W_\square}(x)$ defined analogously: $\mathbf{1}_{2W_\square}(x) = 1$ if $x \in W$ and $\mathbf{1}_{2W_\square}(x) = 0$ for $x \in 2W_\square \setminus W$.

The isotropic PCF $\bar{g}(r)$ can be estimated as the rotational mean of the estimate of $\big(\kappa_2 * g\big)(x)$. From an image processing perspective, the mapping of the estimate of $\big(\kappa_2 * g\big)(x)$ onto a grid is a d-dimensional image with real-valued pixels. The rotational mean is therefore the average of all pixel values at a distance r to the origin.

ESTIMATION OF THE STRUCTURE FACTOR

The PSD $\gamma(\xi)$ is essentially the Fourier transform of the covariance function $\mathrm{cov}_f(x)$,

$$\hat{\kappa}_2(\xi)\cdot\gamma(\xi) = \mathscr{F}\big(\mathrm{cov}_f\big)(\xi), \quad \xi\in\mathbb{R}^d \qquad (8)$$

(Mugglestone and Renshaw, 1996). Therefore, if the support of the covariance function $\mathrm{cov}_f(x)$ is subset of the centered window $\frac{1}{2}(W\oplus(-W))$ then from Eq. 6 it follows that

$$\mathscr{F}\mathrm{cov}_f(\xi) = (2\pi)^{d/2}\mathscr{F}\left(\frac{\bar{\mathscr{F}}\,\mathbb{E}|\hat{f}_W|^2}{c_W}\right)(\xi)$$

for all $\xi\in\mathbb{R}^d$. Again we are setting $\kappa(x)=\mathbf{1}_C(x)/a^d$ for $C=[0,a]^d$, $a>0$ and $\kappa_2=\big(\kappa*\kappa^*\big)(x)$. Then $\hat{\kappa}_2(\xi)\approx(2\pi)^{-d/2}$ for sufficiently small a. As a consequence, the estimator

$$\tilde{s}(\xi) = (2\pi)^d\,\lambda\,\mathscr{F}\left(\frac{\bar{\mathscr{F}}|\hat{f}_W|^2}{c_W}\right)(\xi), \qquad \xi\in\mathbb{R}^d \quad (9)$$

is asymptotically unbiased for $s(\xi)$ for $a\to 0$. A scheme of estimating $s(\xi)$ is given in Fig. 3.

We would like point out that the estimated structure factor $\tilde{s}(\xi)$ ultimately represents a d-dimensional digital image, and consequently the isotropic function $\bar{s}(\rho)$ can be estimated as the rotation mean of the pixel values of $\tilde{s}(\xi)$.

Finally, we remark that alternative estimation procedures for $s(x)$ are discussed by Hawat *et al.* (2023), see also Pinkney *et al.* (2024); Yang and Guan (2026) for regularized spectral estimation using a tapered Fourier transform, where recent developments have introduced multitaper estimators for enhanced accuracy. However, as pointed out by Yang and Guan (2026), multitapering does not fit fast Fourier transform, which comes at the expense of computing time. Furthermore, the multitaper Fourier transform is designed exclusively for cubioidal windows and only leads to an approximate correction of edge effects. In the isotropic case we also refer to Bartlett's estimator of the isotropic structure factor $\bar{s}(\rho)$, which is essentially based on a discrete Fourier-Bessel transform of $\bar{g}(r)$ (Bartlett, 1964). Other estimators investigated by Hawat *et al.* (2023) use the quadrature rules of Ogata (2005) and Baddour and Chouinard (2015), respectively.

SECOND-ORDER CHARACTERISTICS OF THE EXTREMAL POINTS OF BERRY'S WAVE

In the following, we consider a typical Gaussian random field, namely *Berry's random wave* (or *Berry's wave* for short), see e. g. the paper by Estrade and Fournier (2024) and references therein. The sites of the local extrema of Berry's wave form a hard-core point field. Berry's wave is well-suited for case studies because realizations of it can be generated easily and quickly, and the sites of its local extrema can be determined in a straightforward manner. On the other hand, the sites of the local extrema are subject of more recent theoretical investigations. Beliaev *et al.* (2019) calculated, for example, the reduced moment measure of the critical points of Berry's wave using the Kac-Rice formula (Adler and Taylor, 2007), where critical points are understood to be saddles or local extrema. Ladgham and Lachieze-Rey (2023) did this more generally, namely for smooth Gaussian fields, see also Azaïs and Wschebor (2009). We use the methods introduced in the previous sections to estimate the PCF and the structure factor of the local extrema.

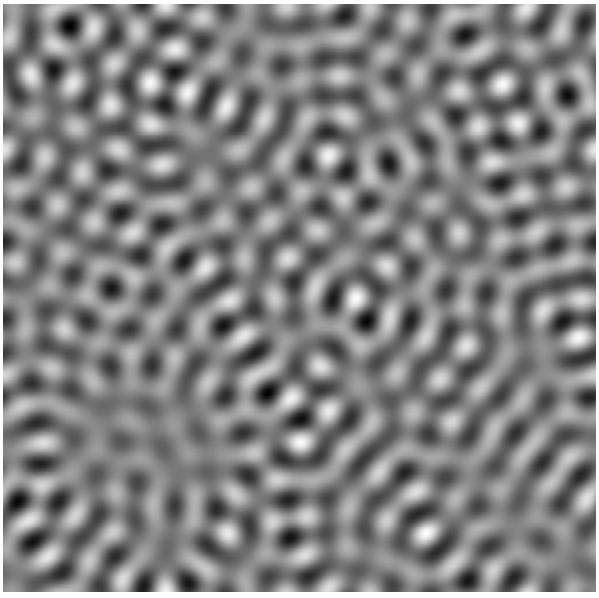

Fig. 4. *A realization* $\Psi^{(m)}(x)$ *of Berry's wave for* $m=4\,096$*, a subimage of* $1\,024\times 1\,024$ *pixels out of totally* $8\,192\times 8\,192$ *pixels of size* $a=1\,\mu\mathrm{m}$*,* $\rho_0=0.1\,\mu\mathrm{m}^{-1}$*,* $r_0=70.156\,\mu\mathrm{m}$ *(about 70 pixels).*

GENERATION OF BERRY'S WAVE

In this section we restrict ourselves to the 2D case. Berry's wave $\Psi(x)$, $x\in\mathbb{R}^2$ is a macroscopically homogeneous and isotropic Gaussian random field

with zero expectation $\mathbb{E}\Psi(x) = 0$, unit variance $\operatorname{var}\Psi(x) = \mathbb{E}\Psi^2(x) = 1$ and the Bessel correlation function

$$\mathbb{E}\Psi(y)\Psi(y+x) = J_0\big(\rho_0\|x\|\big), \qquad x,y \in \mathbb{R}^2$$

for sufficiently large m, where $\rho_0 > 0$ is a parameter of $\Psi(x)$. From

$$\frac{d}{dr}J_0(\rho_0 r) = -\rho_0 J_1(\rho_0 r), \qquad r \geq 0$$

it follows that the local extrema of the correlation function $J_0(\rho r)$ are the zeros of $J_1(\rho_0 r)$, and therefore, the zero $r_0 = 7.015\,587/\rho_0$ is the characteristic distance in $\Psi(x)$.

Realizations of Gaussian random fields can be generated e. g. using the spectral method given by

$$\Psi^{(m)}(x) = \sqrt{\frac{2}{m}}\sum_{k=1}^{m}\cos(u_k + v_k x), \quad x \in \mathbb{R}^2, \qquad (10)$$

where $u_1, \ldots, u_m$ are pairwise independent random numbers uniformly distributed on the interval $[0, 2\pi)$. Furthermore, the $v_1, \ldots, v_m$ are pairwise independent random vectors, whose distribution is determined by the correlation function of the Gaussian random field (Shinozuka and Jan, 1972; Lantuéjoul, 2013).

In the special case of Berry's wave $\Psi(x)$ with the parameter ρ_0, the power spectral density is (up to a multiplicative constant) the function $\delta(\|\xi\| - \rho_0)$, where $\delta(\cdot)$ denotes Dirac's delta function,

$$\frac{1}{2\pi}\int_{\mathbb{R}^2} J_0\big(\rho_0\|x\|\big)\,\mathrm{e}^{-ix\xi}\,dx = \frac{1}{\rho_0}\,\delta\big(\|\xi\| - \rho_0\big), \quad \xi \in \mathbb{R}^2.$$

As a consequence, if the random vectors v_k may be given by $v_k = \rho_0(\cos\varphi_k, sin\varphi_k)$, where $\varphi_1, \ldots, \varphi_m$ are pairwise independent random numbers uniformly distributed on $[0, 2\pi)$, then $\Psi^{(m)}(x) \to \Psi(x)$ as $m \to \infty$. The sampling of a realization $\Psi^{(m)}(x)$ of Berry's wave $\Psi(x)$ on a square lattice forms a digital grey-tone image (with pixel values of type `float`). For our purposes, an image of $8\,192 \times 8\,192$ pixels was generated, see Fig. 4 for a subimage.

EXTREMAL POINTS

The sites of the local extrema of Berry's random wave can be estimated from realizations of $\Psi(x)$ by locally fitting a (slightly reduced) bicubic function to 3×3-environment of the pixels of the image data and computing its local minimum or maximum. The point pattern of Fig. 5 was obtained from the subimage shown in Fig. 4. The total number of the local extrema of the entire image is $m = 123\,780$; the estimated intensity is $\lambda \approx 1.845\,\mathrm{mm}^{-2}$.

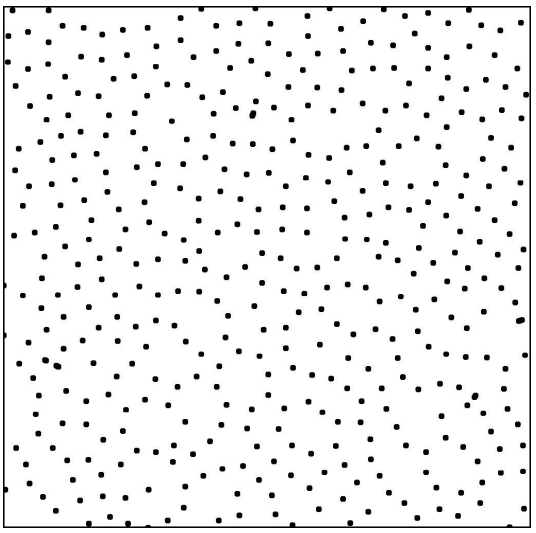

Fig. 5. *Sites of the local extrema of Berry's wave, point pattern obtained from the subimage shown in Fig. 4*

We first show a 2D plot of the estimate of the PCF $g(x)$, which is always obtained as an intermediate result of the estimation via frequency domain, Fig. 6. Clearly, the isotropy of Berry's wave is inherited to the field of its extreme points. Therefore, $g(x)$ is also invariant with respect to rotations about the origin, and it makes sense to calculate the rotation mean given in Fig. 10b.

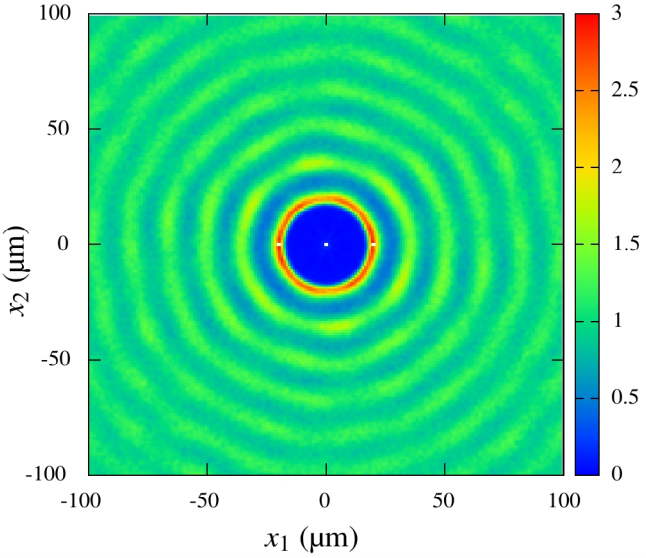

Fig. 6. *Estimate of the PCF $g(x)$ of the extremal points of Berry's wave for $\rho_0 = 0.1\,\mu\mathrm{m}^{-1}$ using Eq. 7 for the width $a = 1\,\mu\mathrm{m}$ of the smoothing kernel $\kappa_2(x)$*

The estimates of the PCF $\bar{g}(r)$ from the estimators Eq. 3 resp. Eq. 7 shown in Fig. 7 are very similar. Differences are mainly due to different regularization

strategies, which are not comparable. While Eq. 3 performs a 1D smoothing of the frequencies of point distances, Eq. 7 smooths the point pattern itself with a 2D kernel. Therefore, the two estimators are difficult to compare from a statistical point of view. However, due to the large point number m, the estimator given by Eq. 7 has computational advantages over the conventional one.

Disregarding the PCF estimates for $0 \leq r < 20\,\mu\text{m}$, which may be a consequence of of the limited number m of iterations in Eq. 10 and misdetections of the local extrema from the realization of Berry's wave, it can be postulated that the local extrema form a hard-core point field with the hard core distance $2/\rho_0$.

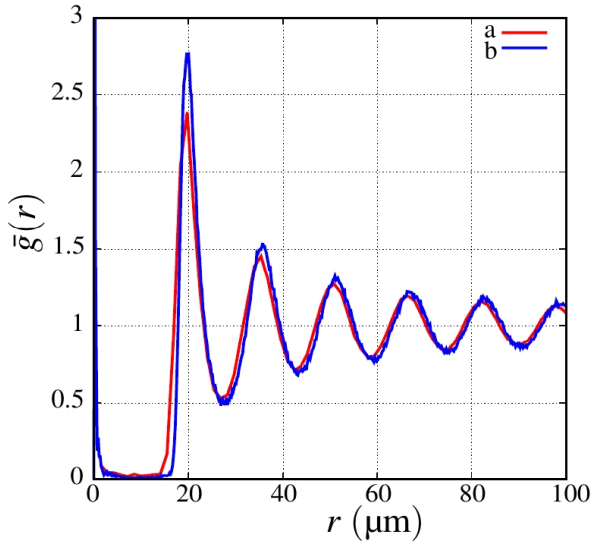

Fig. 7. *Estimates of the PCF $\bar{g}(r)$ of the extremal points of Berry's wave for $\rho_0 = 0.1\,\mu\text{m}^{-1}$: a) using Eq. 3 for the width $\sigma = 2\,\mu\text{m}$ of the Epanechnikov kernel, b) using Eq. 7 for the width $a = 1\,\mu\text{m}$ of the smoothing kernel $\kappa(x)$*

An estimate of the structure factor $\bar{s}(\rho)$ of the extremal points of Berry's wave is shown in Fig. 8. The estimation is based on Eq. 9, where no smoothing is involved. Furthermore, we remark that a similar structure factor was obtained from the Percus-Yevick approximation for random hard spheres packings (Wertheim, 1963), see also the very instructive article Maier *et al.* (2024). The similarities between the random field of the sphere centers of hard sphere packings and the extremal points of Berry's wave lie in the high-energy first interference and the sharp decline in the amplitude of the alternating structure factor $s(\rho)$. Obvious differences between the structure factor of hard spheres packings and that of the extremal points of Berry's wave are as follows: In Fig. 8, there is a discontinuity (probably a pole) at $\rho = 4\rho_0 = 0.4\,\mu\text{m}^{-1}$, and at $\rho = 8\rho_0 = 0.8\,\mu\text{m}^{-1}$, there is obviously a discontinuity in the first derivative. This is not the case for hard spheres packings, even at high packing densities.

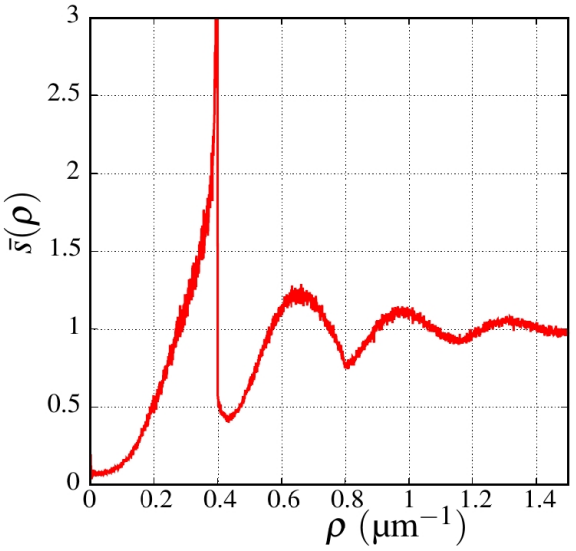

Fig. 8. *Estimate of the structure factor $\bar{s}(\rho)$ of the extremal points of Berry's wave for $\rho_0 = 0.1\,\mu\text{m}^{-1}$*

ON DISTRIBUTION OF FILLER PARTICLES IN RUBBER

During the rubber manufacturing process, for example for tires, globular filler particles (carbon black or silica) are added to a viscous rubber matrix. Stirring and kneading the hot rubber mass leads to a uniform distribution of the particles and their partial dissolution. During subsequent cooling, some of the dissolved carbon or silica precipitates, with the remaining particles acting as nuclei. The complex interplay of dissolution and precipitation determines the particle size distribution and arrangement of the final material and thus its physical and technical properties. In the rubber industry, the particle size distribution is called macro-dispersion; details are specified in industrial standards (ASTM D7723, 2018). Radiometric stereomicroscopy using fresh cuts is one method for estimating the macro-dispersion (Ohser *et al.*, 2019).

This section proposes the characterization of the arrangement of carbon black filler particles in rubber based on tomographic images of solid rubber samples, where the second-order quantities $\bar{g}(r)$ and $\bar{s}(\rho)$ of the particle centers are estimated.

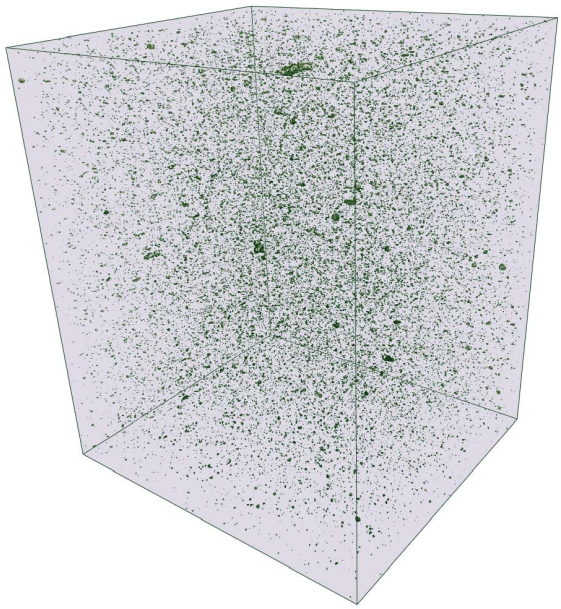

Fig. 9. *Volume rendering of a tomographic image of globular carbon black particles (dark) in a rubber matrix (light), micro-CT, propagation-based phase contrast,* $1\,100 \times 1\,000 \times 1\,300$ *pixels out of totally* $2\,560 \times 2\,560 \times 2\,160$ *cubic pixels of size* $0.64\,\mu\text{m}$.

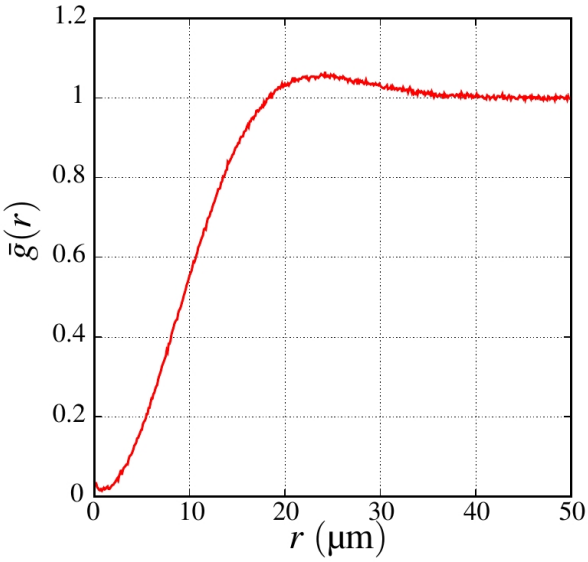

Fig. 10. *Estimate of the PCF* $\bar{g}(r)$ *of the centers of carbon black particles in rubber, estimation via frequency domain, width* $a = 1.28\,\mu\text{m}$ *of the smoothing kernel* $\kappa(x)$

X-ray absorption contrast between carbon black and rubber matrix is, as expected, very low. For this reason, images of sufficiently high contrast must be taken using an alternative contrast mode. The tomographic image shown in Fig. 9 was taken at the beamline ID19 of the European Synchrotron Radiation Facility (ESRF) in Grenoble, France. A photon energy of 35 keV was chosen for limiting potential dose issues to the sample while maintaining sufficient contrast between carbon black and rubber matrix. For further measures to achieve sufficient photon flux density, narrow bandwidth illumination and reduction the wave front modulations see Rack *et al.* (2010). The use of an indirect X-ray image detector ensured a sufficiently high resolution of the projection images. The effective pixel size was 0.64 µm. Additionally, so-called propagation-based phase contrast was applied for edge enhancement (Cloetens *et al.*, 1996), and back-projection was combined with phase-retrieval (Paganin *et al.*, 2002; Weitkamp *et al.*, 2011). The resulting image consists of totally $2\,560 \times 2\,560 \times 2\,160$ pixels, but due to slight shading, only a sub-image of $2\,048 \times 2\,048 \times 2\,048$ pixels from the interior was used in the following.

The segmentation of the carbon black phase was based on the binarization of the image with respect to the Otsu threshold. Subsequent labeling of the connected components (particles) and measurement of their mean breadth (mean Ferret diameter) resulted in the detection of approximately 285 000 particles larger than 2 µm. The centers of gravity were assumed to be the particle centers.

The estimated PCF $\bar{g}(r)$ shown in Fig. 10 exhibits the typical soft-core behavior of the particle centers, which is partly a consequence of the particle size distribution. (The minimum distance between two spherical particles must ultimately be larger than the sum of their radii.) However, this alone does not explain the shape of $\bar{g}(r)$, as the (volume-weighted) mean particle size (about 3.5 µm) and the mean number of particles per unit volume (about $125\,000\,\text{mm}^{-3}$) would be far too small. Another reason for the shape of the PCF is certainly to be found in the complex interplay between the dissolution of carbon black and its subsequent reprecipitation.

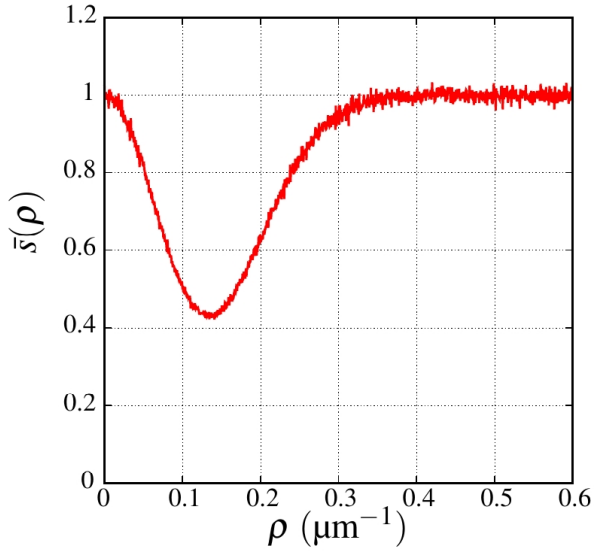

Fig. 11. *Estimates of the structure factor $\bar{s}(\rho)$ of the centers of carbon black particles in rubber*

From an image processing perspective, the function $1-\bar{g}(r)$ looks like the kernel of a Laplace-of-Gaussian (LoG) filter (Jähne, 2005), a typical bandpass filter, which is also known as the *Marr-Hildreth* operator. The bandpass characteristic is almost ideally expressed in the structure factor $\bar{s}(\rho)$, Fig. 11. In fact, $1-\bar{s}(\rho)$ is – up to a multiplicative constant – similar the transfer function of the LoG filter. Compared to the structure factor of the Poisson point field (Fig. 2a), the energy in the mid-frequency band is substantially suppressed.

SUMMARY AND DISCUSSION

Based on ideas originally attributed to MS Bartlett, the spectral measure Γ of random point fields, its density γ, and finally the structure factor s are introduced, where s contains the same information about a point field as the PCF g. Statisticians usually prefer interpreting point patterns based on estimates of the PCF g, while physicists are often more familiar with the structure factor s obtained through diffraction experiments. We think it might be insightful to consider both functions, g and s.

This article presents a method for estimating the PCF g via the frequency domain, incorporating regularization of estimation and correction of edge effects. Of course, estimating the PCF via the frequency domain is only advantageous for large point numbers. At that point, statistical problems become less significant, while numerical aspects, such as the required computation time and software performance, play an increasingly important role. In this context, it is worth recalling that a random point field is nothing more than a special case of a random set or a random function whose auto-correlation function can only be efficiently estimated via the frequency domain.

We would like to emphasize once more the regularization of the estimation. While the conventional method given by Eq. 3 convolves (smooths) in the domain of point distances, the method given by Eq. 7 convolves the point pattern itself. The latter is achieved naturally by mapping the point pattern onto a regular grid, with the grid spacing controlling the regularization. The method for estimating the structure factor s given by Eq. 9 initially does not involve any regularization. For our purposes, namely estimating s for the extremal points of Berry's wave or the carbon black particles in rubber, this is, in our opinion, not necessary. However, suitable smoothing can easily be integrated into the estimation procedure, e.g., by multiplying the covariance function cov_f by the transfer function of a smoothing kernel, cf. Fig. 3.

Finally, we would like point out that as an intermediate result of estimation via frequency domain, the PCF is initially obtained as a function of both the distance and the direction of the point pairs, see e. g. Fig. 6. This allows for characterizing macroscopically homogeneous but anisotropic point fields.

ACKNOWLEDGEMENT

This article is dedicated to my former colleague Prof. Konrad Sandau, who passed away on October 13, 2025, at the age of 75. Konrad Sandau was a long-standing member of the ISSIA.

DATA AVAILABILITY STATEMENT

In this study, no new data was generated or analyzed.

REFERENCES

Adler RJ, Taylor J (2007). Random Fields and Geometry. New York: Springer.

ASTM D7723 (2018). Standard Test Method for Rubber Property – Macro-Dispersion of Fillers in Compounds. ASTM International, West Conshohocken, PA.

Azaïs J, Wschebor M (2009). Level Sets and Extrema of Random Processes and Fields. Hoboken, NJ: Wiley & Sons.

Baddeley AJ, Rubak E, Turner R (2015). Spatial Point Patterns. Methodology and Applications with R. Boca Raton, FL: Chapman & Hall/CRC.

Baddeley A. T, Davies M, Hazelton ML (2025). An improved estimator of the pair correlation function of a spatial point process. Biometrika 112:asaf021.

Baddour N, Chouinard U (2015). Theory and operational rules for the discrete Hankel transform. J Opt Soc Amer A 32:611–22.

Bartlett MS (1963). The spectral analysis of point processes. J R Stat Soc B25:264–96.

Bartlett MS (1964). The spectral analysis of two-dimensional point processes. Biometrika 51:299–311.

Bartlett MS (1975). The statistical analysis of spatial patterns. Monogr. Appl. Prob. Statist. London: Chapman & Hall.

Beliaev D, Cammarota V, Wigman I (2019). Two-point function for critical points of a random plane wave. Int Math Res Notes 2019:2661–89.

Boudjemâa A (2023). A charged Coulomb Bose gas with dipole-dipole interactions. Phys Letters A 465:128712.

Brémaud P (2014). Fourier-Analysis & Stochastic Processes. New York: Springer.

Brémaud P, Massoulié L (2002). Power spectra of general shot noises and Hawkes point processes with a random excitation. Adv Appl Prob 34:205–22.

Chiu SN, Stoyan D, Kendall WS, Mecke J (2013). Stochastic Geometry and Its Application, 3rd Ed. Chichester: Wiley.

Cloetens P, Barrett R, Baruchel J, Guigay JP, Schlenker M (1996). Phase objects in synchrotron radiation hard X-ray imaging. J Phys D Appl Phys 29:133–46.

Coppens P (2006). The structure factor. International Tables of Crystallography B, Chapter 1.2:10–24.

Daley DJ, Vere-Jones D (1988). An introduction to the theory of point processes. New York: Springer.

Estrade A, Fournier J (2024). Gaussian fields through geometrical properties. Hal archives ouvertes-04481440:1–50.

Fiksel T (1988). Edge-corrected density estimators for point processes. Statistics 19:67–76.

Gabrielli A, Torquato S (2004). Voronoï and void statistics for superhomogeneous point processes. Phys Rev E Stat Nonlin Soft Matter Phys :041105.

Graham I (1980). Spectral analysis and distance methods in the study of archaeological distributions. J Archaeol Sci 7:105–29.

Grainger JP, Rajala TA, Murrell DJ, Olhede SC (2025). Spectral estimation for point processes and random fields. Biometrika 103:asaf089.

Hawat D, Gautier G, Bardenet R, Lachièze-Rey R (2023). On estimating the structure factor of a point process, with applications to hyperuniformity. Statist Comp 33:hal–03615250v2.

Jähne B (2005). Digital Image Processing, 6th Ed. Berlin, Heidelberg: Springer.

Kittel C (2018). Introduction to Solid State Physics. Hoboken, NJ: J. Wiley & Sons.

Koch K (2002). Spektralanalyse zufälliger abgeschlossener Mengen. Universität Siegen: Diploma Thesis.

Koch K, Ohser J, Schladitz K (2003). Spectral theory for random closed sets and estimating the covariance via frequency space. Adv Appl Prob 35:603–13.

Ladgham S, Lachieze-Rey R (2023). Local repulsion of planar Gaussian critical points. Stoch Proc Appl 166:104221.

Lantuéjoul C (2013). Geostatistical Simulation – Models and Algorithms. Berlin: Springer.

Le HH, Illisch S, Radusch HJ, Steinberger H (2008). Macro- and microdispersion of carbon black in liquid silicone rubbers. Plastics Rubber Composites 37:367–75.

Maier JD, Gaus K, Wagner J (2024). Measurable structure factors of dense dispersions containing polydisperse optically inhomogeneous particles. J Appl Crystallogr 57:1503–13.

Massaro M, del Campo A (2025). Spatial form factor for point patterns: Poisson point process, Coulomb gas, and vortex statistics. Phys Rev Res 7:023107.

Matérn B (2013). Spatial Variation, 2nd Ed. Lecture Notes in Statistics, Vol. 36. New York: Springer Science & Business Media.

Mugglestone M, Renshaw E (1996). A practical guide to the spectral analysis of spatial point processes. Comp Statist Data Analysis 21:43–65.

Oberhettinger F (1972). Tabeles of Bessel Transforms. New York, Heidelberg, Berlin: Springer.

Ogata H (2005). A numerical integration formula based on the Bessel functions. Publ RIMS Kyoto Univ 41:949–70.

Ohser J, Lacayo-Pineda J, Putman M, Rack A, Dobrovolskij D (2019). Estimation of filler macro-dispersion in rubber matrix by radiometric stereo microscopy. J Microsc 274:32–44.

Ohser J, Mücklich F (2000). Statistical Analysis of Microstructures in Materials Science. Chichester, New York: J Wiley & Sons.

Ohser J, Schladitz K (2009). 3D Images of Materials Structures – Processing and Analysis. Weinheim, Berlin: Wiley VCH.

Ohser J, Schladitz K, Koch K, Nöthe M (2005). Diffraction by image processing and its application in materials science. Z Metallkunde 96:731–7.

Paganin D, Mayo SC, Gureyev TE, Miller PR, Wilkins SW (2002). Simultaneous phase and amplitude extraction from a single defocused image of a homogeneous object. J Microscopy 206:33–40.

Pinkney C, Euán C, Gibbert A, Shojaie A (2024). Regularised spectral estimation for high-dimensional point processes. arXiv240312908 :preprint.

Poularikas AD (2000). The Transforms and Applications Handbook, 2. Ed. Boca Raton, FL: CRC Press.

Prémaud P, Massoulié L, Ridolfi A (2005). Power spectra of random spike fields and related processes. Adv Appl Prob 37:1116–46.

Rack A, García-Moreno F, Schmitt C, Betz O, Cecilia A, Ershov A, Rack T, Banhart J, Zabler S (2010). On the possibilities of hard X-ray imaging with high spatio-temporal resolution using polychromatic synchrotron radiation. J X Ray Sci Tech 18:429–41.

Rajala TA, Olhede SC, Grainger JP, Murrell DJ (2023). What is the Fourier transform of a spatial point process? IEEE Trans Inf Theory 69:5219–52.

Ripley BD (1976). The second-order analysis of stationary point processes. J Appl Prob 13:255–66.

Shinozuka M, Jan CM (1972). Digital simulation of random processes and its application. J Sound Vibration 25:111–28.

Stoyan D, Kendall W, Mecke J (1985). Stochastic Geometry and Its Applications, 1st Ed. Chichester: J. Wiley & Sons.

Vere-Jones D (1974). An elementary approach to the spectral theory of stationary random measures. In: Harding EF, Kendall DG, eds., Stochastic Geometry. Chichester: J. Wiley & Sons, 307–21.

Walters JK, Honeybone PJR, Huxley DW, Newport RJ, Howells DS (1993). A high-resolution neutron-diffraction study of the structure of amorphous hydorgenated carbon, a-c:h. J Phys Condens Matter 5:L387–L392.

Weitkamp T, Haas D, Wegrzynek D, Rack A (2011). *ANKAphase*: software for single-distance phase retrieval from inline X-ray phase-contrast radiographs. J Synchrotron Radiation 18:617–29.

Wertheim M (1963). Exact solution of the Percus-Yevick integral equation for hard spheres. Phys Rev Letters 10:321–3.

Yang J, Guan Y (2026). Fourier analysis of spatial point processes. Bernoulli 32:370–92.